scientific reports

Check for updates

OPEN

Flexible hybrid self-powered piezo-triboelectric nanogenerator based on BTO-PVDF/PDMS nanocomposites for human machine interaction

Wentao Dong[1], Mengyun Li[1], Chang Chen[1], Kun Xie[2], Jinhua Hong[3]✉ & Lin Yang[4]✉

As flexible and wearable electronics play more and more important role in smart watches, smart glass and virtual reality, and the power supply to the wearable electronics have been revealed more attentions for long-term usage and continuous healthy monitoring. To overcome the challenge, flexible self-powered BTO-PVDF/PDMS piezoelectric-triboelectric electric hybrid generators (BPP-HNG) are developed to human gesture monitoring and human machine interaction (HMI) application without external power supply. BPP-HNG based on BTO-PVDF and PDMS films are prepared by sol–gel and spin-coating method. When the BTO content is 20 wt.%, BPP-HNG exhibits better electrical performance with an output voltage of 20.51 V. A real-time gesture monitoring system is designed and developed to human machine interaction, which is able to control the motion of robot finger through BPP-HNG. BPP-HNG could monitor and recognize various gestures in real time, enabling synchronization between the human hand and the robot's hand. With the convergence of AI technology and big data, BPP-HNG based HMI technology is expected to realize the potential of smarter and more intuitive interactions.

Keywords Wearable electronics, Hybrid piezoelectric-triboelectric nanogenerator, BTO-PVDF/PDMS nanocomposites, Human machine interaction, Gesture monitoring

Flexible and wearable electronics have been widely applied to daily life and industrial applications[1–3], such as smart watches[4], health monitoring bracelets[5], and virtual reality glasses[6], which are adopted to interact with the digital world due to high degree of convenience and versatility[7–9]. However, the long-term usage of the flexible and wearable electronics for with multi-sensing functionality is limited with the energy consumption[10,11]. It would be more challenging and demanding to study flexible self-powered electronics to provide sustainable and energy support to enhance their performance and practicality.

Self-powered sensors convert environmental energy and human movement energy into electrical energy, which could provide potential solution to power supply to flexible sensors[12,13]. Nanogenerator technology has received widespread attention as an emerging energy harvesting technology[14,15], which offers a promising approach to harvest various forms of ambient energy, including mechanical, vibrational, and thermal energy, and converting them into usable electrical power[16,17]. Pan et al. developed a straightforward, transparent, highly sensitive, and high power-density electronic skin based on a triboelectric nanogenerator (S-TENG), for harvesting energy from the human body and real-time monitoring of physiological motion status[18]. Chen et al. developed a flexible, wearable piezoelectric sensor by electrospinning a fluorinated polyimide (FPI) nanofiber membrane and packaging it with FPI resin. The sensor effectively detects bending and pressure signals, making it suitable for motion and pressure monitoring[19]. Single-effect nanogenerators exhibit unstable output power and low energy conversion efficiency in practical applications[20]. These limitations significantly impair its performance in high-power-demand scenarios, hindering its practical applicability[21,22]. For example, piezoelectric sensors are able to

[1]School of Electrical and Automation Engineering, East China Jiaotong University, Nanchang 330013, China. [2]Department of Civil and Environmental Engineering, Transportation Informatics Lab, Old Dominion University (ODU), 4635 Hampton Boulevard, Norfolk, VA 23529, USA. [3]School of Advanced Manufacturing, Nanchang University, Nanchang 330031, China. [4]Department of Mechanical and Electrical Engineering, Huazhong Agricultural University, Wuhan 430070, China. ✉email: hjh@ncu.edu.cn; lin.yang@hzau.edu.cn

recognize different gesture actions by detecting the movement of finger joints, but the piezoelectric properties of piezoelectric materials are usually low, resulting in insufficient sensitivity of the sensor[23–25]. Therefore, hybrid self-powered nanogenerator should be studied to improve the output electrical performance.

Energy harvesting efficiency could be improved for providing more reliable and stable power supply by integrating diverse energy conversion mechanisms[26]. The existing hybrid nanogenerators include: piezoelectric and triboelectric composite[27], piezoelectric and electromagnetic composite[28], triboelectric and thermoelectric composite. Hybrid piezoelectric-triboelectric nanogenerator integrates piezoelectric and triboelectric effects, which has higher energy collection efficiency, simple material and structure, and easy integration. Song et al. reported a novel self-supporting structure hybrid triboelectric/piezoelectric nanogenerator (TPNG) to harvest low-frequency and low-amplitude mechanical energy through friction and deformation, which can be used as a self-powered sensor to reflect changes in pressure[29]. Chen et al. proposed a hybrid piezoelectric/triboelectric nanogenerator (PT-NG) based on a composite thin film to achieve the coupling of piezoelectric charge generation and triboelectrification at the same time to improve energy conversion efficiency[30]. Although it is important for hybrid piezoelectric/triboelectric nanogenerators to improve energy conversion efficiency, it still faces complex structure, insufficient flexibility, unstable energy output, and insensitivity to changes in the external environment, which limits their long-term application in human gesture recognition.

Flexible self-powered sensor with piezoelectric-triboelectric effect could be applied to gesture recognition and human machine interaction (HMI) application[31–33]. Wu et al. designed a multi-functional hybrid electronic skin (TPES) integrated by a piezoelectric capacitive pressure sensor (PCPS) and a triboelectric nanogenerator (TENG), which enables integration with man-computer interaction (HCI) module to achieve gesture recognition and material perception HCI systems[34]. Zhang et al. present a human–computer interaction system consisting of triboelectric nanogenerators (PTSM-TENGs) based on an ionic hydrogel (PTSM) prepared from polypropylene amine (PAM), tannic acid (TA), sodium alginate (SA), and MXene. The system extracts and analyzes the multidimensional signal features of PTSM-TENGs to realize gesture visualization, robot hand control and object recognition[35]. HMI based on flexible self-powered sensors significantly expand the potential applications of wearable devices such as education, entertainment, and healthcare[36–38]. Flexible self-powered sensor should be developed to more natural human machine interaction with external actuators friendly.

Due to its excellent bending and deformation capabilities, flexible self-powered BTO-PVDF/PDMS piezoelectric-triboelectric electric hybrid generators (BPP-HNG) is laminated onto the surface of the human finger and follow the bending motion of human finger. BTO-PVDF/PDMS nanocomposites could record the deformation signal of human finger, which could be used as human machine interface to control the motion of the robot finger. The main contributions of this work are in the two-folds:

(1) Flexible self-powered BPP-HNG is prepared to gesture recognition and human machine interaction. BPP-HNG has the better output performance with an output voltage of 20.51 V, when the BTO content is 20 wt.%, the thickness of BTO-PVDF film is 7 μm, and nylon is used as the positive electrode material. It improves the efficiency of the energy conversion performance of BPP-HNG and opens up new possibilities for the energy supply and self-power sensing of wearable electronic devices.

(2) BPP-HNG has been applied to human gesture detection and human machine integration successfully. A gesture monitoring and human machine interaction platform based on BPP-HNG is built to recognize different gestures and control the motion of robot fingers. It has recognized 10 predefined human gestures by BPP-HNG laminated onto the surface of human fingers, which is applied to control the motion of the robot fingers.

The main work is arranged as the following: Design and principle of flexible self-powered BPP-HNG with multi-layer structure are illustrated in Sect. "Design and principle". Section "Materials and fabrication" shows that material selection and fabrication process of BPP-HNG. X-ray diffractometry (XRD) pattern as well as the surface morphology of BTO-PVDF films with different BTO ratios are tested to devote the influencing factors about the output performance of BPP-HNG in Sect. "Results and discussion". Flexible self-powered BPP-HNG with BTO-PVDF/PDMS nanocomposites is applied to human gesture detection and human machine interaction in Sect. "Conclusion and discussion", which is applied to control the motion of robotic finger through BPP-HNG for collecting the corresponding motion signal of the human finger. Finally the whole work is summarized.

Design and principle

BTO-PVDF nanocomposite films are prepared using BTO doped into PVDF to increase the piezoelectric properties of the films, and then the composite films were directly embedded into the surface of non-flexible PDMS films to form BTO-PVDF/PDMS composite films. This composite film is utilized to prepare BTO-PVDF/PDMS piezoelectric-triboelectric electric hybrid generators (BPP-HNG) with sandwich-structure. The incorporation of the BTO-PVDF composite film significantly enhances the surface roughness of the PDMS film, thereby improving triboelectric charge generation. Meanwhile, the PDMS matrix provides structural protection to the BTO-PVDF nanofibers, facilitating the generation of piezoelectric charges during compressive deformation and ensuring the composite film produces stable and durable electrical signals. The BPP-HNG combines both piezoelectric and triboelectric effects to produce higher power output than the TENG and PENG devices alone. It also functions as a self-powered sensor for detecting various signals from finger movements, recognizing various gestures and human motion detection, and even for manipulating robotic fingers.

Figure 1a shows the schematic diagram of BPP-HNG laminated onto the surface of human finger for continuous signal measurement of human gesture. BPP-HNG is designed with multilayer structure: Cu electrode, BTO-PVDF/PDMS composite film, rubber spacer (Ecoflex), nylon film and Cu film from the bottom to the top. Cu film is used as the electrode and nylon material as the tribo-positive electrode. Cu electrode is connected to the bottom of the BTO-PVDF/PDMS composite film, the other Cu electrode is connected to the tribo-positive material (nylon fabric), and they are connected with a rubber spacer (Ecoflex) of 2 mm.

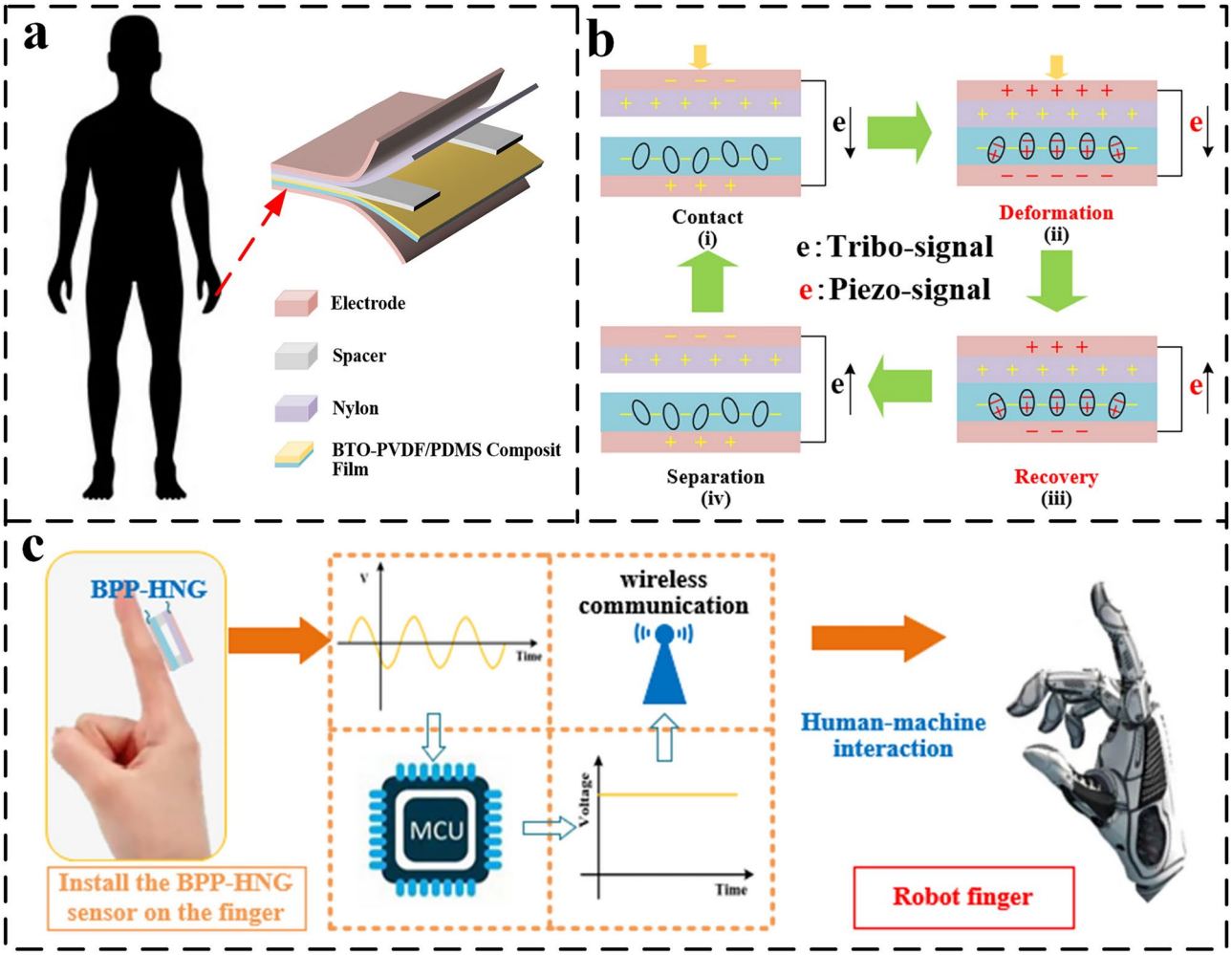

Fig. 1. The schematic diagram of a hybrid piezoelectric-triboelectric nanogenerator (BPP-HNG) based on BTO-PVDF/PDMS for human machine interaction applications. (**a**) BPP-HNG with multi-layer structure for human gesture monitoring; (**b**) The working principle of BPP-HNG; (**c**) Schematic diagram of the application process of BPP-HNG for controlling the motion of robot finger remotely.

Figure 1b demonstrates the working mechanism of the BPP-HNG with the hybrid piezoelectric and triboelectric effects. The generation of triboelectric electricity is attributed to the coupling of the triboelectric effect (contact charging) and the electrostatic induction effect, while the charges and potential difference would be generated between the bottom and top surface of the piezoelectric BTO-PVDF film during the bending process of the piezoelectric film. In BPP-HNG, the nylon layer acts as a tribo-positive electrode and PDMS acts as a tribo-negative electrode. Based on the triboelectric series, nylon exhibits a tendency to donate electrons, whereas PDMS tend to accept electrons. As a result, the nylon generates a positive triboelectric charge, while the BTO-PVDF/PDMS composite film generates the same amount of charge with opposite polarities on the surface. In the initial state, without any external force or contact between the BTO-PVDF/PDMS composite film and the nylon triboelectric material, no charge is generated in BPP-HNG. When an external force is applied, Fig. 1b(i) shows the nylon layer begins to move in the direction of contact with the BTO-PVDF/PDMS composite film. The positive and negative charges are induced respectively on the upper and lower surfaces of the copper electrodes of BPP-HNG due to the electrostatic induction effect. Due to the triboelectric effect, the nylon loses electrons to be positively charged, while the BTO-PVDF/PDMS composite film gains electrons to be negatively charged. The potential difference drives electrons to flow through the external load, generating an instantaneous frictional current. After the contact friction is energized, the nylon layer returns to its initial position and the BPP-HNG starts to work. When the two layers are in complete contact, the positive and negative triboelectric charges are completely balanced by the electrostatic induction charges. However, the external force does not disappear, and BPP-HNG undergoes deformation, which induces the piezoelectric charge by BTO-PVDF composite film and a piezoelectric current is generated through an external circuit (Fig. 1b(ii)). Figure 1b(iii) shows the induced piezoelectric charge would be also recovered and the opposite piezoelectric current is generated, when the external force disappears, BTO-PVDF undergoes a brief recovery process. The nylon layer begins to move back to its initial position and the accumulated triboelectric charge is returned through the external load (Fig. 1b(iv)). The electrostatic voltage is generated until the two layers are completely separated. Throughout the circle of the

deformation and recovery process, the triboelectric and piezoelectric signals are synergistically combined to enhance the output electrical performance of BPP-HNG.

BPP-HNG laminated onto the surface of human finger for hand gesture detection and human machine integration. Figure 1c shows the control process of robot finger by BPP-HNG with the microcontroller unit (MCU) and wireless communication system. BPP-HNG is installed on the finger, and a real-time human–machine interaction is carried out by controlling the manipulator through the microsystem. The robot finger is successfully controlled by human finger with BPP-HNG.

Materials and fabrication

Material selection and manufacturing processes play an important role in the mechanical and electrical properties of BPP-HNG. The materials for BPP-HNG are prepared as: N, N dimethylformamide (DMF, AR, 99.5%), polyvinylidene difluoride (PVDF) powder, tetragonal phase barium titanate powder (BaTiO3, BTO, 99.5%, < 4 μm), anhydrous ethanol (C2H6O, AR, 95%), deionized water, and PDMS (Sylgard184 silicone elastomers), which was used as a mixture of non-viscous prepolymer and curing agent (ratio 10:1), these materials are all purchased from shanghai Aladdin Biomedical Technology Co., Ltd.

Figure 2a shows the preparation process of BPP-HNG, including the mixing of BTO-PVDF solution, the spin coating, curing and stripping process of BTO-PVDF composite film, the preparation of BTO-PVDF/PDMS composite film and the assembly of BPP-HNG. ITO glass substrate (5 cm × 5 cm) is cleaned ultrasonically in ethanol solution for 3–5 min, followed by rinsing with deionized water and drying in an oven at 50–80 °C for 20 min to remove any residual moisture. Figures 2a(i) and a(ii) depict the preparation of BTO-PVDF composites. Firstly, 0.5 g of BTO nanoparticles are weighed and dissolved in 16 mL of DMF solvent (8 mL of DMF per gram of PVDF powder), and the mixture is ultrasonicated for 30 min. Subsequently, 2 g of PVDF powder is slowly added to the DMF solution containing BTO nanoparticles. The resulting mixture is continuously stirred at 70 °C for 1 h to form a uniform BTO-PVDF composite viscous solution. During the process, the temperature of the solution should not exceed a certain threshold (around 100 °C), and the addition of PVDF powder should be slow to prevent the agglomeration of PVDF particles. To investigate the effect of BTO nanoparticle content on

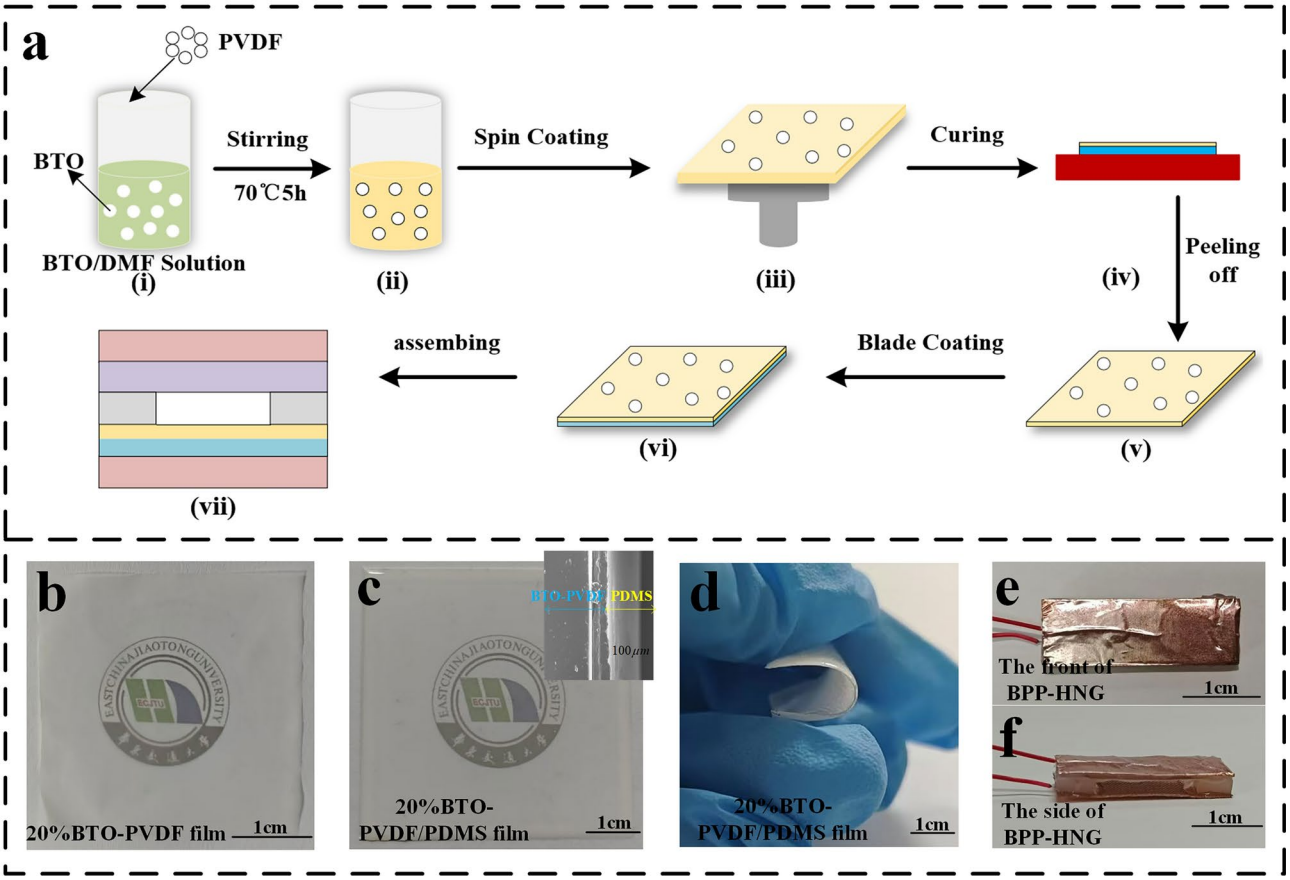

Fig. 2. Preparation process of BPP-HNG and corresponding optical picture. (**a**) Fabrication process of BTO-PVDF composite film; Optical images of (**b**) 20 wt.% BTO-PVDF composite films and (**c**) 20 wt.% BTO-PVDF/PDMS composite film with SEM image (top right); (**d**) Optical image of 20 wt.% BTO-PVDF/PDMS composite film in the bended format; Optical images of the assembled BPP-HNG in (**e**) the front and (**f**) the side formats.

the output performance of flexible BTO-PVDF composite film, BTO-PVDF composite viscous solutions with BTO contents of 0, 5, 10, 15, 20, and 25 wt.% are prepared in the same manner, respectively.

Figures 2a(iii) and a(iv) show the preparation of BTO-PVDF composite film. The ITO glass substrate is fixed on the rotating tray at the center of the homogenizer. A rubber-tipped dropper is then used to place 6 to 8 drops of the prepared BTO-PVDF composite viscous solution onto the substrate, which is rotated at 500 rps for 40 s to obtain the BTO-PVDF composite wet film. To investigate the thickness effect on the output performance of the piezoelectric nanogenerator, different thicknesses samples of BTO-PVDF composite films are obtained by adjusting the rotational speeds (500, 1000, 1500, and 2000 rps). BTO-PVDF composite film is heated in a drying oven at 120 °C for 4 min. After curing, the film is carefully removed from the glass substrate to yield the BTO-PVDF composite piezoelectric film. Figures 2a(v) and (vi) demonstrate the preparation of BTO-PVDF/PDMS composite film. The PDMS is poured onto the horizontally PVDF composite film, and the excess PDMS was scraped off (with a weight ratio of PDMS base material to cross-linking agent of 10:1) to form a smooth composite film. The BTO-PVDF/PDMS mixture was then cured for 4 h at 60 °C to obtain the composite film.

Figures 2b and c depict the transparent composite films of 20 wt.% BTO-PVDF and 20 wt.% BTO-PVDF/PDMS, respectively. The school logo is clearly visible through BTO-PVDF/PDMS films with good transparency. The top-right panel of Fig. 2c presents the cross-sectional Scanning Electron Microscopy (SEM) image of BTO-PVDF/PDMS, revealing that the BTO-PVDF nanofibers and PDMS silicone rubber are firmly bonded. Figure 2d shows the optical image of the BTO-PVDF/PDMS composite under bending conditions, indicating its good flexibility. BPP-HNG is fabricated and assembled as follows: (1) 50 μm thick copper foils is placed on one side of the PVDF-BTO/PDMS composite film(30 mm × 10 mm) and on one side of the nylon fabric (30 mm × 10 mm); (2) a 2 mm thick rubber spacer (ecoflex) with a hollow structure is placed between the BTO-PVDF/PDMS composite film and the nylon fabric to form a cavity structure; (3) the BTO-PVDF/PDMS composite film, copper electrode, spacer layer, and nylon fabric are stacked and assembled in sequence to fabricate the BPP-HNG. Figures 2e-f show the optical images of the assembled BPP-HNG in the front and the side formats.

Results and discussion

XRD measurement of crystal structure

The crystal structure of the prepared BTO-PVDF composites with varying BTO contents is characterized using X-ray diffractometry (XRD, RWS-01-I, Shimadzu corporation Co., Ltd., Japan), and the corresponding data is shown in Fig. 3a. The XRD patterns of the composite films with 0 wt.%, 5 wt.%, 10 wt.%, 15 wt.%, 20 wt.%, and 25 wt.% BTO contents are presented from bottom to top. In the XRD pattern of PVDF (0 wt.% BTO), a distinct β-phase diffraction peak is observed at $2\theta = 20^{\circ}$, indicating that the composite film exhibits piezoelectric properties. The XRD patterns of BTO-PVDF composite films exhibit characteristic diffractometry peaks corresponding to the tetragonal phase of BTO nanoparticles and the β-phase of PVDF, indicating that both the BTO nanoparticles and PVDF in the composite films possess piezoelectric properties.

SEM analysis of flexible composite films

Figures 3b exhibits that Scanning Electron Microscopy (SEM, SU8010, Hitachi Co., Ltd., Japan) is employed to observe the surface morphology of BTO-PVDF composite films with varying BTO contents (0 wt.%–25 wt.%) and the cross-section of BTO-PVDF/PDMS. Figure 3 shows that with increasing BTO content, a higher density of BTO particles is observed on the surface. Consequently, additional two-phase interfaces are formed between

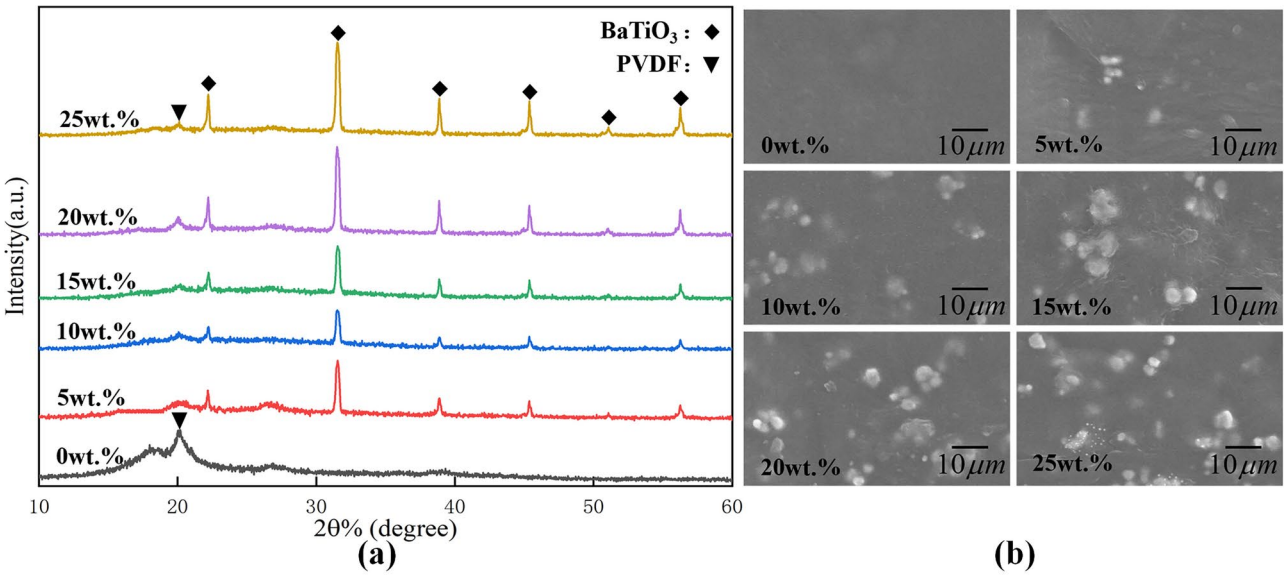

Fig. 3. XRD patterns (**a**) and SEM surface topography (**b**) of BTO-PVDF composite films with different BTO contents.

the BTO nanoparticles and the PVDF matrix, facilitating polarization and enhancing the output performance and stability of the composite film. At 25 wt.% BTO content, the BTO nanoparticles increase significantly, the particle spacing decreases, and agglomeration occurs, leading to a weakened interfacial polarization effect and a reduction in the piezoelectric output of the film.

Performance of BPP-HNG

Output performance of BPP-HNG would be tested to improve the practical applications: energy harvesting, self-powered sensing, and various intelligent systems. Comprehensive assessment of BPP-HNG is implemented to analyze the output voltage of BPP-HNG under varying conditions. Different materials, pressures, and other relevant factors are adopted to test the output performance of BPP-HNG. To enhance the piezoelectric performance, the piezoelectric film is prepared by doping BTO into PVDF solution with variant BTO contents. Figure 4a shows that the output voltages of BPP-HNG are recorded under the same excitation with different BTO contents. The output voltage of the BPP-HNG firstly increases as the BTO content from 0 wt.% to 20 wt.% and then decreases as the BTO content from 20 wt.% to 25 wt.%, indicating that optimal performance (output voltage about 12.15 V) of BPP-HNG is achieved when the BTO content is approximately 20 wt.%. The thickness of the BTO-PVDF composite film also affects the output performance of BPP-HNG. To investigate the influence of film thickness, BTO-PVDF composite films with different thicknesses are prepared by varying the homogenizer rotational speed. Thicknesses of BTO-PVDF composite films 7 μm, 5 μm, 3 μm, and 1 μm are achieved at 500,

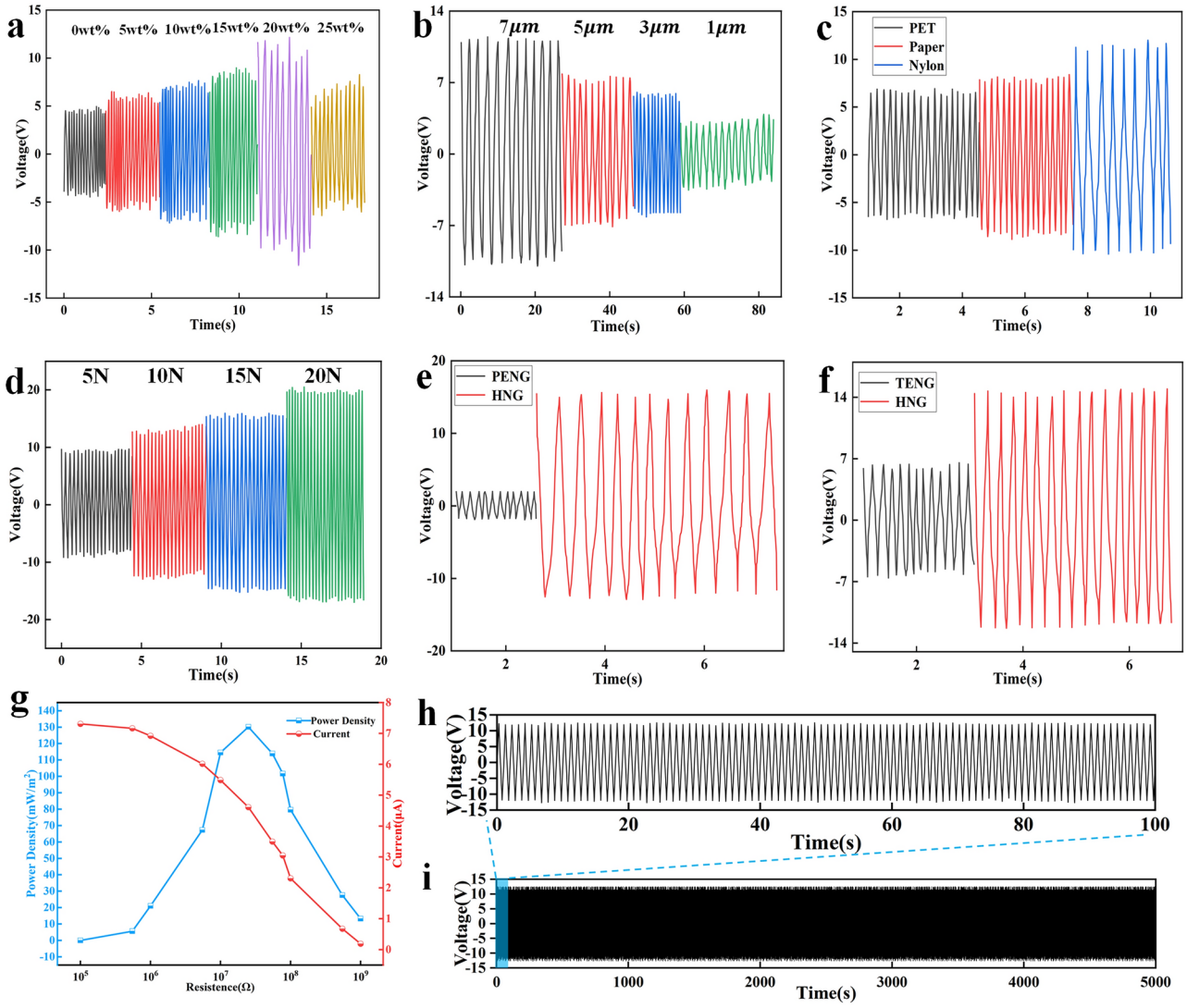

Fig. 4. Output electrical performance of BPP-HNG under different external conditions. (**a**) Output voltages of BPP-HNG with different BTO contents; (**b**) Output voltages of BPP-HNG with different BTO-PVDF thicknesses; (**c**) Output voltages of BPP-HNG with different cathode materials; (**d**) Output performances of BPP-HNG under different pressures; Comparison of the output performances of (**e**) PENG and BPP-HNG; and (**f**) TENG and BPP-HNG; (**g**) The output current and power density of BPP-HNG under different loads; (**h**) Initial 100 cycles; (**i**)Stability test of the BPP-HNG.

1000, 1500, and 2000 rps, respectively. Figure 4b exhibits that the thickness of the composite film decreases with the increasing rotational speed, resulting in a decreasing output voltage of BTO-PVDF composite films. When the film thickness is 7 μm, the output voltage of BPP-HNG is approximately 11.47 V.

In addition to the aforementioned factors, the type of friction positive electrode material also influences the electrical output performance of the BPP-HNG. Three different positive electrode materials: PET, paper, and nylon are adopted to test the performance of BPP-HNG. Figure 4c presents that the output voltage (about 12 V) of BPP-HNG is higher when nylon is used as the positive electrode material, which is consistent with the triboelectric series. Among these materials, nylon is selected as friction electrode material for subsequent studies. Figure 4d shows the output performance of BPP-HNG under varying pressures (5 N, 10 N, 15 N, and 20 N). The output voltage of the BPP-HNG increases with the external increasing pressure. The output voltage is maximum when the pressure is 20 N, and the peak voltage is about 20.51 V. Piezoelectric nanogenerator (PENG) with BTO-PVDF composite films, and triboelectric nanogenerator (TENG) with PDMS films, were prepared to compare their energy conversion performance with that of the BPP-HNG. Figure 4e shows that output voltage of the BPP-HNG is higher than PENG, and Figure 4f shows output voltage of the BPP-HNG is higher than that of TENG. It is indicated the BTO-PVDF and PDMS composite enhances the output performance of BPP-HNG. It is found that when the doping concentration of BTO is 20%, the output voltage of the sensor reaches the peak. In order to evaluate the electrical performance at this doping concentration more comprehensively, the current output of the sensor under different load conditions was further measured, and the corresponding power density was calculated. Figure 4g clearly shows the variation of the current output and power density of the sensor with the load at the optimal doping level. The maximum power density of 130.12 mW/m^2 can be obtained when BPP-HNG is 25MΩ. Figure 4h shows 100 initial cycles. Figure 4i shows the output performance of BPP-HNG under 5000 cycles of continuous operation. The results show that BPP-HNG has no obvious performance degradation within 5000 cycles, indicating that it can maintain stable output performance. Therefore, the maximum output voltage and current (20.51 V, 0.86μA) can be obtained when a hybrid nanogenerator is constructed using an ideal composite film. Supplementary Table S1 online reports the comparison of the output performance of the device proposed in this work with previous similar materials[39–42]. In contrast, the device proposed in this work has a streamlined structure and exhibits excellent output performance. In these studies, the performance of nanogenerators has been significantly improved by optimizing the material combination, innovating the structural design and improving the preparation process, which has promoted the development of this field. By compounding different materials, not only the piezoelectric properties of the materials are improved, but also good mechanical stability and machinability are maintained, so that they show better output performance under high load conditions. In terms of structural design, innovative designs such as multi-layer composite structure and fiber structure are adopted to further enhance the piezoelectric and triboelectric effects, achieve higher voltage output and power density, and demonstrate its potential in high-power demand applications. By optimizing the preparation process, the performance and consistency of the material are further improved, which makes the material have better reliability and repeatability in practical applications, and shows great potential in applications such as wearable devices and human–computer interaction.

BPP-HNG for HMI

Human machine interaction (HMI) has been revealed more and more significant attentions, and more intelligent and convenient HMI methods have been introduced with flexible sensors, which could be laminated onto the curved surface of human body. Human machine interaction system with various perception, feedback, and control mechanisms should be designed to interact between humans and robots more naturally. Human gesture-monitoring and human machine interaction system based on flexible BPP-HNG is developed to real-time gesture monitoring and human machine interaction. Figure 5a presents the experimental setup of the human machine interaction system, including flexible gloves with BPP-HNG, an STM32 microcontroller, a data processing module, a Bluetooth module, and a robotic finger, and other components. The experiment gloves were fabricated using nitrile gloves with five 5 cm × 1 cm BPP-HNG attached to each finger joint. When the user's hand movement occurs, the BPP-HNG flexible glove collects the corresponding electrical signals. The weak electrical signals are amplified using the signal amplifier section in the data processing module to ensure that they are processed within the appropriate voltage range; the negative half-week is removed by the rectifier module to ensure the positivity of the signals; and the filter module further removes the high-frequency noise to ensure the clarity of the signals. The STM32 microcontroller is utilized to extract the key information from the processed signals to ensure the quality of the signals and to provide initial feature extraction. The Bluetooth module is then used to send the processed signals from the previous microcontroller to the latter microcontroller, which performs further feature extraction and generates control instructions robot finger movements based on these signals. The structural block diagram of human machine interaction system is illustrated in Fig. 5b.

Figure 5c illustrates that the HMI system was employed to evaluate the interaction of ten distinct gestures, which the flexible glove with different BPP-HNGs on each finger could be worn on the human finger. BPP-HNG could collect the bending signal of human finger, which could follow the bending process of the human finger. BPP-HNG exhibits excellent bending properties and conforms effectively to the contours of human finger joints during flexion. As the finger bends, the BPP-HNG tracks the finger's motion, generating voltage changes that reflect the movement of individual fingers and control the corresponding robotic fingers. Figure 5d depicts the waveform signal recorded by BPP-HNG with single channel, and it has a distinct combination of waveform characteristics during the bending process for each BPP-HNG on the different fingers.

This property offers considerable advantages for the recognition of various gestures. Figure 5e shows the robotic fingers are fully synchronized and successfully controlled by the human fingers worn with flexible glove with BPP-HNGs during the interaction process. Figure 5f depicts the Waveform signals corresponding to the five gestures in Fig. 5e. When the human hand performs an action, the robotic hand executes the corresponding

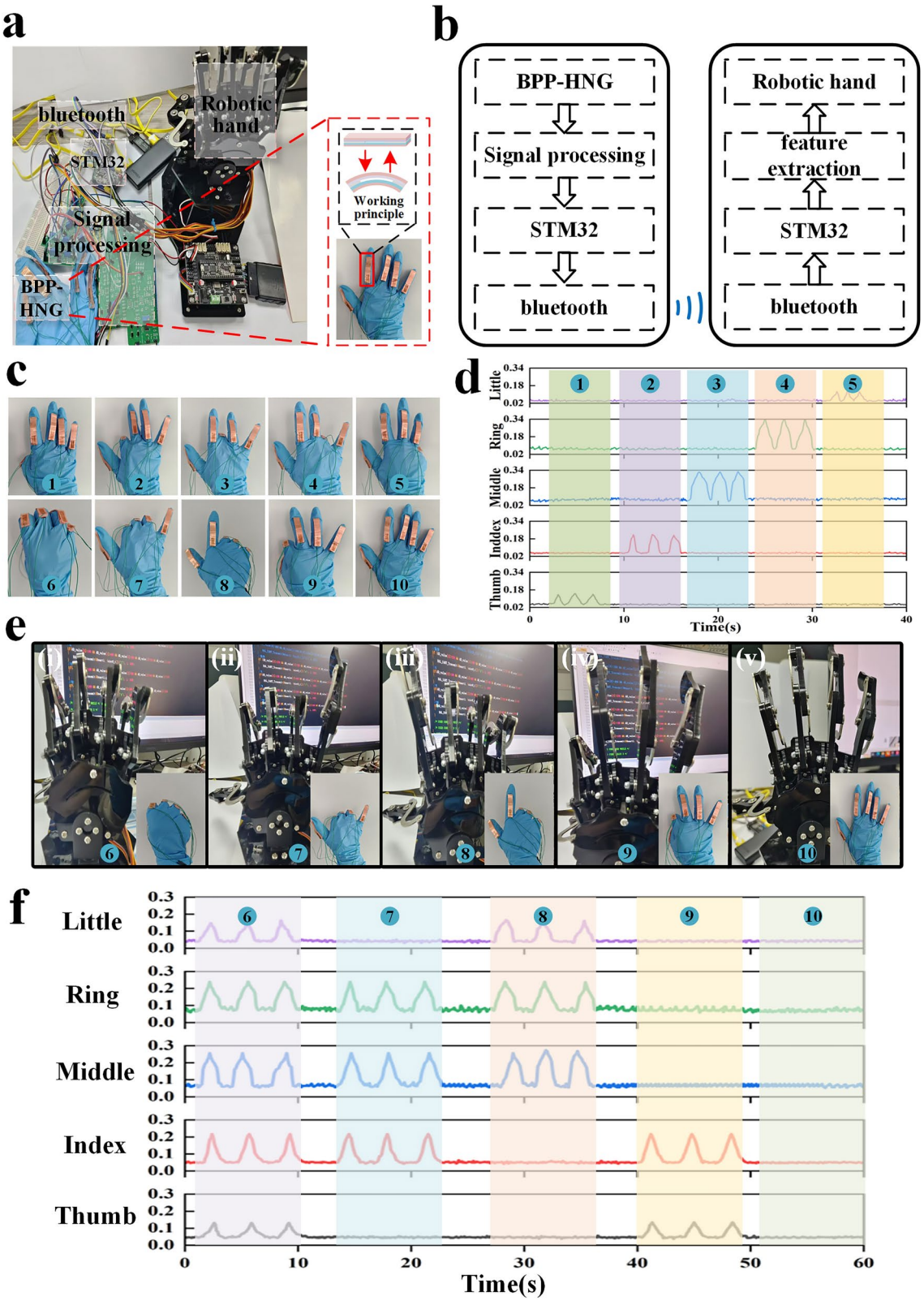

Fig. 5. Human machine interaction based on BPP-HNG for the motion control of robot finger remotely. (**a**) Experiment platform for human machine interaction based on human finger with BPP-HNG and robot finger; (**b**) Block diagram of human machine interaction system with BPP-HNG for the motion control of robot finger; (**c**) Ten different postures of human finger with BPP-HNG; (**d**) Waveform signal recorded by BPP-HNG with single channel; (**e**) Real-time gesture interaction diagrams of the robotic finger controlled by human finger with BPP-HNG; (**f**) Waveform signals corresponding to the five gestures in (**e**).

action. Supplementary Videos 1 and 2 online demonstrate the process of controlling a robotic hand for gesture interaction. It demonstrates the potential application of wearable human machine interaction based on flexible BPP-HNG could be applied to different fields. Human machine interaction based on gesture interaction with flexible BPP-HNG is characterized by its intuitive, natural, and convenient features. It enhances accessibility for individuals with disabilities through precise gesture recognition technology, promoting the development of immersive experiences such as virtual and augmented reality.

Conclusion and discussion

Flexible self-powered BPP-HNG based on piezoelectric-friction electric mechanism has been integrated into the flexible glove, which is applied to human gesture monitoring and human machine interaction for control the motion of robot finger. Flexible BPP-HNG follow the deformation signal of human finger for more accurate signal recording of bending process of human finger. The main work was concluded as:

(1) Flexible self-powered BPP-HNG based on piezoelectric-friction electric hybrid nanogenerator was prepared to gesture recognition and human machine interaction. A BTO-PVDF piezoelectric nanocomposite film was fabricated by embedding onto the surface of a triboelectrically charged PDMS film for enhancing triboelectric properties. PDMS matrix with its high mechanical strength provided structural protection for the BTO-PVDF composite film during compressive deformation. The BTO-PVDF composite film exhibits both piezoelectric and triboelectric effects with the highest output voltage of about 20.51 V, when the BTO content was 20 wt.%, the thickness of the BTO-PVDF film was 7 μm, and nylon was used as the positive electrode material.

(2) Flexible BPP-HNG based human gesture monitoring and human machine interaction system was built to control the motion of robot finger remotely. It had recognized 10 predefined human gestures by BPP-HNG laminated onto the surface of human fingers. The robotic finger could follow the motion of human finger in real time, providing a viable strategy for the design of human machine interaction systems, enabling more natural, high-precision, and real-time interactions.

BPP-HNG has been successfully applied human machine interaction and control the motion of robot finger. With development of material, fabrication and information technology, it could be improved in several aspects:

(1) Advanced data processing technology and intelligent algorithms are integrated into the flexible BPP-HNG to recognize and predict human gestures and movements for more intelligent human–computer interaction.

(2) Integrating other types of sensors such as temperature, pressure, and biosensors into the flexible BPP-HNG enables the construction of multimodal interaction systems that provide a richer and more natural interaction experience to the users.

Data availability

Data is provided within the manuscript and Data will be made available on request. The corresponding author should be contacted if someone wants to request the data from this study.

Received: 18 January 2025; Accepted: 28 April 2025
Published online: 08 May 2025

References

1. Hu, J. & Dong, M. Recent advances in two-dimensional nanomaterials for sustainable wearable electronic devices. *J. Nanobiotechnol.* **22**, 63 (2024).
2. Wu, Y. H., Li, Y. W., Tao, Y., Sun, L. Y. & Yu, C. Y. Recent advances in the material design for intelligent wearable devices. *Mater. Chem. Front.* **7**, 3278–3297 (2023).
3. Li, P. et al. A scalable, robust and high sensitivity fiber sensor for real-time body temperature monitoring. *Soft Sci.* https://doi.org/10.20517/ss.2024.60 (2025).
4. Tian, H. et al. Electrochemical sensing fibers for wearable health monitoring devices. *Biosensors Bioelectronics* **246**, 115890 (2024).
5. Ma, X. G. Analysis of Human Exercise Health Monitoring Data of Smart Bracelet Based on Machine Learning. *Comput. Int. Neurosci.* **2022**, 1 (2022).
6. Lau, S. T. et al. Enhancing professional competency in clinical procedures using head-mounted display virtual reality - a mixed method study. *Med. Educ. Online* **28**, 2232134 (2023).
7. Chen, R. P. et al. Applications of MXenes in wearable sensing: Advances, challenges, and prospects. *Mater. Today* **75**, 359–385 (2024).
8. Dong, W. T., Yang, L., Gravina, R. & Fortino, G. ANFIS fusion algorithm for eye movement recognition via soft multi-functional electronic skin. *Inf. Fusion* **71**, 99–108 (2021).
9. Kim, K. H., Kim, J. H., Ko, Y. J. & Lee, H. E. Body-attachable multifunctional electronic skins for bio-signal monitoring and therapeutic applications. *Soft Sci.* https://doi.org/10.20517/ss.2024.09 (2024).
10. Liu, Y. C. et al. Cascaded MXene/Metal-Organic framework system enables rapid gelation of ultrastretchable and high-toughness conductive hydrogels for multifunctional wearable electronics. *Chem. Eng. J.* **503**, 158288 (2025).
11. Zhong, S. J. et al. Passive Isothermal Flexible Sensor Enabled by Smart Thermal-Regulating Aerogels. *Adv. Mater.* https://doi.org/10.1002/adma.202415386 (2025).
12. Hu, H. L. & Zhang, F. Rational design of self-powered sensors with polymer nanocomposites for human-machine interaction. *Chin. J. Aeronaut.* **35**, 155–177 (2022).
13. Liu, S.-Z., Guo, W.-T., Zhao, X.-H., Tang, X.-G. & Sun, Q.-J. Self-powered sensing for health monitoring and robotics. *Soft Sci.* https://doi.org/10.20517/ss.2024.65 (2025).
14. Shao, Y. C. et al. Nanogenerator-based self-powered sensors for data collection. *Beilstein J. Nanotechnol.* **12**, 680–693 (2021).
15. Dong, W. T. et al. Stretchable Self-Powered TENG Sensor Array for Human-Robot Interaction Based on Conductive Ionic Gels and LSTM Neural Network. *IEEE Sens. J.* **24**, 37962–37969 (2024).
16. Zhao, T. M. et al. Wearable biosensors for real-time sweat analysis and body motion capture based on stretchable fiber-based triboelectric nanogenerators. *Biosensors Bioelectronics* **205**, 114115 (2022).
17. Kim, M. J. et al. Wearable fabric-based ZnO nanogenerator for biomechanical and biothermal monitoring. *Biosensors Bioelectronics* **242**, 115739 (2023).

18. Pan, J. et al. A noval transparent triboelectric nanogenerator as electronic skin for real-time breath monitoring. *J. Colloid Interface Sci.* **671**, 336–343 (2024).
19. Chen, S. et al. Fluorine polyimide nanofibrous composites with outstanding piezoelectric property for human motion monitoring. *Chem. Eng. J.* **502**, 157320 (2024).
20. Lv, Y. et al. An ultraweak mechanical stimuli actuated single electrode triboelectric nanogenerator with high energy conversion efficiency. *Nanoscale* **14**, 7906–7912 (2022).
21. Gao, Y. K. et al. Spontaneously established reverse electric field to enhance the performance of triboelectric nanogenerators via improving Coulombic efficiency. *Nat. Commun.* https://doi.org/10.1038/s41467-024-48456-1 (2024).
22. Chandrasekar, J. et al. In-situ oxidized MXene dopes for enhanced sensitivity of PVDF piezoelectric nanogenerators in Morse code transmission and photocatalysis applications. *Mater. Today Energy* **48**, 101760 (2025).
23. Park, H., Gbadam, G. S., Niu, S. M., Ryu, H. & Lee, J. H. Manufacturing strategies for highly sensitive and self-powered piezoelectric and triboelectric tactile sensors. *Intl. J. Extreme Manuf.* **7**, 012006 (2025).
24. Zhong, S. J. et al. Metal-based nanowires in electrical biosensing. *Rare Met.* **43**, 6233–6254 (2024).
25. Zhou, Y. et al. Microscopic Response Mechanism of Epsilon-Negative and Epsilon-Near-Zero Metacomposites. *Research* **8**, 0556 (2025).
26. Huang, F.-C., Sun, X.-D., Shi, Y. & Pan, L.-J. Textile electronics for ubiquitous health monitoring. *Soft Sci.* https://doi.org/10.20517/ss.2024.37 (2024).
27. Yousry, Y. M. et al. Theoretical Model and Outstanding Performance from Constructive Piezoelectric and Triboelectric Mechanism in Electrospun PVDF Fiber Film. *Adv. Func. Mater.* https://doi.org/10.1002/adfm.201910592 (2020).
28. Wang, L. et al. Smart nodding duck: A hybrid Halbach electromagnetic piezoelectric self-powered sensor for smart fisheries. *Chem. Eng. J.* **493**, 152694 (2024).
29. Song, C., Xia, K. & Xu, Z. A self-supported structure hybrid triboelectric/piezoelectric nanogenerator for bio-mechanical energy harvesting and pressure sensing. *Microelectron. Eng.* **256**, 111723 (2022).
30. Chen, Q. et al. Hybrid Piezoelectric/Triboelectric Wearable Nanogenerator Based on Stretchable PVDF-PDMS Composite Films. *ACS Appl Mater Interfaces* **16**, 6239–6249 (2024).
31. Nie, Z. X., Yu, Y. & Bao, Y. Application of human-computer interaction system based on machine learning algorithm in artistic visual communication. *Soft. Comput.* **27**, 10199–10211 (2023).
32. Dong, W. T., Yang, L. & Fortino, G. Stretchable Human Machine Interface Based on Smart Glove Embedded With PDMS-CB Strain Sensors. *IEEE Sens. J.* **20**, 8073–8081 (2020).
33. Dong, W. T., Yang, L., Gravina, R. & Fortino, G. Soft Wrist-Worn Multi-Functional Sensor Array for Real-Time Hand Gesture Recognition. *IEEE Sens. J.* **22**, 17505–17514 (2022).
34. Wu, S. et al. Convolutional Neural Networks-Motivated High-Performance Multi-Functional Electronic Skin for Intelligent Human-Computer Interaction. *Nano Energy* **122**, 109313 (2024).
35. Zhu, W. X. et al. Multi-Effects Coupled Nanogenerators for Simultaneously Harvesting Solar, Thermal, and Mechanical Energies. *Adv. Mater. Technol.* https://doi.org/10.1002/admt.202300212 (2023).
36. Ding, Y., Huang, L.-Z., Ji, X.-X. & Ma, M.-G. Utilizing electrospinning to fabricate porous polyvinylidene fluoride/cellulose nanocrystalline/MXene films for wearable pressure sensors. *Int. J. Biol. Macromol.* **284**, 138106 (2025).
37. Chen, Z. H., Qu, C. M., Yao, J. J., Zhang, Y. L. & Xu, Y. Two-Stage Micropyramids Enhanced Flexible Piezoresistive Sensor for Health Monitoring and Human-Computer Interaction. *ACS Appl. Mater. Interfaces.* **16**, 7640–7649 (2024).
38. Huang, C. L., Xiao, M. Y., Li, Z. H., Fu, Z. H. & Shi, R. Bioinspired breathable biodegradable bioelastomer-based flexible wearable electronics for high-sensitivity human-interactive sensing. *Chem. Eng. J.* **486**, 150013 (2024).
39. Shin, S.-Y., Saravanakumar, B., Ramadoss, A. & Kim, S. J. Fabrication of PDMS-based triboelectric nanogenerator for self-sustained power source application. *Int. J. Energy Res.* **40**, 288–297 (2016).
40. Chen, G., Chen, G., Pan, L. & Chen, D. Electrospun flexible PVDF/GO piezoelectric pressure sensor for human joint monitoring. *Diamond Related Mater.* **129**, 109358 (2022).
41. Sahu, M. et al. Piezoelectric Nanogenerator Based on Lead-Free Flexible PVDF-Barium Titanate Composite Films for Driving Low Power Electronics. *Crystals* **11**, 85 (2021).
42. Thakur, V. N. & Han, J. I. Combined Triboelectric and Piezoelectric Effect in ZnO/PVDF Hybrid-Based Fiber-Structured Nanogenerator with PDMS: Carbon Black Electrodes. *Polymers (Basel)* **14**, 4414 (2022).

Acknowledgements

The authors acknowledge supports from the National Natural Science Foundation of China (52165069), Natural Science Foundation of Jiangxi Province (20224BAB214051, 20232BAB214045), China Postdoctoral Science Foundation (2024M750895), and Jiangxi Province Graduate Innovation Special Fund Project Support (YC2024-S427), Urgently needed overseas talent project of Jiangxi Province (20242BCE50081, 20242BCE50050).

Author contributions

W. D., M. L., and L. Y. conceived the experiments, M. L., C. C. conducted the experiments, W. D., M. L, K. X., and J. H. analysed the results, W. D., J. H., and L. Y. discussed the results. All authors reviewed the manuscript.

Declarations

Competing interests

The authors declare no competing interests.

Additional information

Supplementary Information The online version contains supplementary material available at https://doi.org/10.1038/s41598-025-00686-z.

Correspondence and requests for materials should be addressed to J.H. or L.Y.